

# Phase Mapping of Composition-Spread $\text{Fe}_{1-x}\text{Ni}_x$ Binary Alloys

Y. S. Chu,<sup>1</sup> J. D. Almer,<sup>1</sup> D. C. Mancini,<sup>1</sup> Y. K. Yoo,<sup>2</sup> T. Ohnishi,<sup>3</sup> X.-D. Xiang<sup>4</sup>

<sup>1</sup> Advanced Photon Source, Argonne National Laboratory, Argonne, IL, U.S.A.

<sup>2</sup> Intematix Corporation, Moraga, CA, U.S.A.

<sup>3</sup> Ginston Laboratory, Stanford University, Palo Alto, CA, U.S.A.

<sup>4</sup> Stanford Research Institute International, Menlo Park, CA, U.S.A.

## Introduction

The study of structural and physical property relationships has been always at the center of materials science. Traditionally, the mapping of structural and physical properties as function of material composition was accomplished through the synthesis and analysis of samples with discrete compositions prepared one at a time. This process is quite laborious and limited in compositional parameters, which may subsequently miss important opportunities in material discovery. Combinatorial material synthesis,<sup>1</sup> combined with rapid characterization techniques that are currently being developed at SRI-CAT, addresses this issue through continuous mapping of physical or chemical properties as functions of composition for a given system. In this report, we present a phase mapping of continuous  $\text{Fe}_{1-x}\text{Ni}_x$  binary alloy system using x-ray diffraction.

## Methods and Materials

In order to produce a composition-spread  $\text{Fe}_{1-x}\text{Ni}_x$  binary alloy system, three periods of graded Fe/Ni multilayered films were deposited onto an  $\text{Al}_2\text{O}_3(0001)$  substrate at room temperature using a combinatorial ion-beam-sputtering deposition system, as shown in Fig. 1. A linear thickness gradient was achieved using computer-controlled precision mobile masks. Subsequently, as-grown multilayered films were annealed at  $600^\circ\text{C}$  for 3 hours in ultrahigh vacuum ampoules to obtain full precursor mixing normal to the film plane to achieve alloy phase formation. The homogeneity of the alloying phase normal to the substrate and the linearity of the concentration gradient were confirmed by Auger depth-profile analysis. The details of the sample preparation can be found in Ref. 2. The crystal structure of the binary alloy system was mapped using x-ray diffraction with a  $50 \times 50 \mu\text{m}$  beam. The measurements were carried out in air at 2-BM and 1-BM of SRI-CAT using a standard four-circle diffractometer.

## Results and Discussion

The composition-spread sample exhibited two different crystal symmetries (see Fig. 2A). The Ni-rich alloys crystallized into the FCC  $\gamma$ -phase, while the Fe-rich alloys crystallized into the BCC  $\alpha$ -phase. The structural phase transition between the  $\gamma$ -phase and the  $\alpha$ -phase occurs around  $x = 0.12$  with a rather broad two-phase overlap range from  $x = 0.08$  to  $0.18$ . Both structures were found to be "rotationally" epitaxial to the underlying sapphire (0001) substrate. The observed epitaxial relations were  $[111]_\gamma//[0001]_{\text{sub}}$  plus  $[\bar{1}\bar{1}\bar{0}]_\gamma//[\bar{1}\bar{1}\bar{0}]_{\text{sub}}$  for the  $\gamma$ -phase, and  $[110]_\alpha//[0001]_{\text{sub}}$  plus  $[1\bar{1}0]_\alpha//[1120]_{\text{sub}}$  for the  $\alpha$ -phase. However, due to the stacking faults and twin-structure formation, there exist six and twelve symmetric-equivalent rotated domains for the

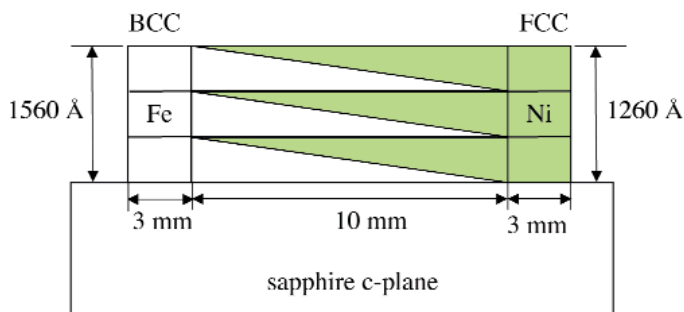


FIG. 1. Preparation of composition-spread  $\text{Fe}_{1-x}\text{Ni}_x$  binary alloy system. Three sets of graded Fe/Ni bilayer were deposited onto  $\text{Al}_2\text{O}_3(0001)$  with an ion-beam sputter deposition and annealed at  $600^\circ\text{C}$  for 3 hours to achieve alloying formation.

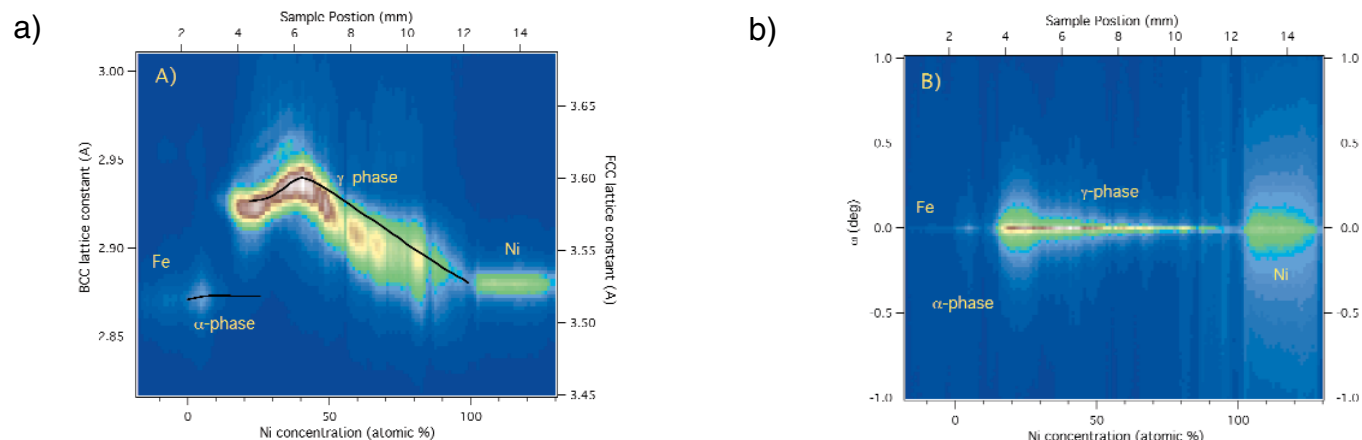


FIG. 2. a) X-ray intensity map of the specular diffraction pattern of  $\text{Fe}_{1-x}\text{Ni}_x$ . The intensity map was constructed by a series of  $q_\perp$  scans at  $100\text{-}\mu\text{m}$  sampling intervals with the beam footprint of  $50 \mu\text{m}$  across the gradient direction (corresponding to  $0.5\%$  composition variation within the sampling area). The solid black line is the previously reported lattice constants from the discrete composition samples, measured at  $15^\circ\text{C}$ .<sup>3</sup> b) The intensity map of the specular texture. The map was constructed by a series of  $\omega$ -rocking scans through the specular reflections of the pure Fe phase,  $\alpha$ -phase,  $\gamma$ -phase and the pure Ni phase as indicated.

$\gamma$ - and  $\alpha$ -phase, respectively. A typical in-plane mosaic ( $\phi$ -rocking width, FWHM) was about  $3\sim 5^\circ$  for all values of  $x$ .

In order to quantify the structural change as a function of composition, we measured the lattice parameters by performing the radial scans along the surface-normal and in-plane directions. Due to the limitation of the four-circle diffraction geometry with its diffraction plane restricted in the vertical plane, the best sampling resolution ( $50\ \mu\text{m}$ ) was achieved only for the mapping of the specular diffraction pattern, and we focus our discussion on the specular diffraction pattern shown in Fig. 2A. The specular diffraction pattern consists of a (110) reflection from BCC structures (pure Fe and  $\alpha$ -phase alloys) and a (111) reflection from FCC structures (pure Ni and  $\gamma$ -phase alloys). In contrast to the rather broader in-plane mosaics of  $3\sim 5^\circ$ , the specular reflections exhibited much better texture as shown in Fig. 2B, with the  $\omega$ -rocking widths (FWHM) better than  $0.1^\circ$  for all values of  $x$ . The intensity variation seen in Fig. 2A with respect to composition is due to the differences in texture with respect to the composition. For example, the Fe-rich alloys and the pure Fe phase have much weaker intensities due to the poorer texture.

While the measured lattice constants for the pure Fe and Ni phase remain constant, the lattice constants of the  $\text{Fe}_{1-x}\text{Ni}_x$  system exhibit complicated dependence on the sampling positions and consequently on the alloying compositions. In order to compare our results, the previously reported lattice constants from the discrete composition samples<sup>3</sup> are plotted together in solid lines. Our data from the composition-spread binary alloy system reproduce all the important features in the lattice constant-composition curve. For example, the phase transition from BCC to FCC in bulk samples does not occur abruptly, similar to our observation. Moreover, the local maxima and the inflection point observed in bulk sample studies are also reproduced in our data.

Our data, however, do present some minor quantitative discrepancies. For example, the phase transition starts at slightly lower Ni concentration in our composition-spread sample compared with the previous data obtained from bulk samples. This can be attributed to the stabilizing effect of the  $\gamma$ -phase at lower Ni concentration because the hexagonal symmetry of the substrate is likely to lower the interfacial energy of the FCC structure of the  $\gamma$ -phase. In addition, the lattice constants measured from our composition-spread sample are consistently smaller in the range of  $x = 0.1\text{--}0.9$ , indicating the full relaxation of the lattice constant was not achieved due to the strain of the film. Moreover, our data exhibit some deviation from the linear decrease of lattice

constant over  $x = 0.5\text{--}0.9$ . However, similar deviations were not observed in the  $q_{\parallel}$  mapping of the (200) and (111) reflections (data not shown), suggesting that this deviation is not due to the particularly poorer linearity in the composition gradient. One likely reason for the deviation is the large residual strains present in this region of the sample. The extent of strain in the film is evident from the broadening of the diffraction peak. In particular, the peak width at  $x = 0.6\text{--}0.8$  is 2–3 times broader than the other region of the Ni concentration and 4 times larger than that of the pure Ni phase. Careful analysis of the residual strain is currently in progress.

## Conclusion

Our data from the continuous  $\text{Fe}_{1-x}\text{Ni}_x$  binary-alloy system demonstrate good overall agreement with the bulk data taken from Fe-Ni alloys of discrete compositions, providing convincing evidence that combinatorial synthesis can be efficiently used for property-structure mapping. However, it is also important to address the differences between the combinatorial thin films and the discrete bulk samples. We attributed some of the discrepancies to the interfacial influence of the substrate and the residual strains on the film. Some of the discrepancies can also be attributed to the differences in relative stability of the alloys. And measurements of phase separation and homogeneity in composition on a much smaller length scale ( $< 1$  micron) are needed.

## Acknowledgments

Use of Advanced Photon Source was supported by the U.S. Department of Energy, Office of Science, Office of Basic Energy Science, under Contract No. W-31-109-Eng-38. The combinatorial material synthesis was partially supported by DARPA, Contract No. MIPR98-0765 through the U.S. Department of Energy under Contract No. DE-AC03-76SF00098.

## References

- <sup>1</sup> X.-D. Xiang, X. Sun, G. Briceno, Y. Lou, K.-A. Wang, W.G. Wallace-Freedman, S.W. Chen, and P.G. Schultz, *Science* **268**, 1738-1740 (1995).
- <sup>2</sup> Y.K. Yoo, T. Ohnishi, G. Wang, F. Duewer, and X.-D. Xiang, Y.S. Chu, D.C. Mancini, Y.-Q. Li, and R.C. O’Handley, manuscript accepted in *Intermetallics*.
- <sup>3</sup> R.M. Bozorth, *Ferromagnetism* (D. Van Nostrand Co., New York, 1951).